Research article

JGS
Journal of the Geological Society

https://doi.org/10.1144/jgs2022-178 | Vol. 180 | 2023 | jgs2022-178

A detective duo of apatite and zircon geochronology for East Avalonia, Johnston Complex, Wales

Anthony J. I. Clarke[1]*, Christopher L. Kirkland[1] and Stijn Glorie[2]

[1] Timescales of Mineral Systems Group, School of Earth and Planetary Sciences, Curtin University, GPO Box U1987, Perth, WA 6845, Australia
[2] Department of Earth Sciences, University of Adelaide, Adelaide, South Australia 5000, Australia
AJIC, 0000-0002-0304-0484; CLK, 0000-0003-3367-8961; SG, 0000-0002-3107-9028
* Correspondence: 20392091@student.curtin.edu.au

Abstract: The Johnston Complex represents a rare inlier of the Neoproterozoic basement of southern Britain and offers a window into the tectonomagmatic regime of East Avalonia during the assembly of Gondwana. This work presents *in situ* zircon (U–Pb, Lu–Hf), apatite (U–Pb), and trace element chemistry for both minerals from the complex. Zircon and apatite yield a coeval crystallization age of 570 ± 3 Ma, and a minor antecrystic zircon core component is identified at 615 ± 11 Ma. Zircon Hf data imply a broadly chondritic source, comparable to Nd data from East Avalonia, and T_{DM}^2 model ages of *c.* 1.5 Ga indicate source extraction during the Mesoproterozoic. Zircon trace element chemistry is consistent with an ensialic calc-alkaline continental arc setting and demonstrates that magmatism was ongoing prior to terrane dispersal at 570 Ma. Apatite trace element chemistry implies a sedimentary component within the melt consistent with voluminous S-type granite production during the formation of Gondwana. The similarity of the εHf and geochemistry between both zircon age populations suggest derivation from a uniform source that did not undergo significant modification between 615–570 Ma. Time-constrained apatite–zircon chemistry addresses complexities in dating S-type granitoids (zircon inheritance) and permits inferences on post-magmatic thermal histories.

Supplementary material: Zircon U–Pb, Lu–Hf and trace element data, and apatite U–Pb and trace element data are available at https://doi.org/10.6084/m9.figshare.c.6484464

Received 14 December 2022; **revised** 8 March 2023; **accepted** 11 March 2023

The assembly of Gondwana from 800 to 550 Ma (Meert and Van Der Voo 1997) coincides with a crucial time in the evolution of Earth systems. Neoproterozoic lithologies provide evidence for the emergence of complex multicellular life (Shen *et al.* 2008), global glaciation (Shields-Zhou *et al.* 2016) and an important period of continental crust production during the Pan-African Orogeny (Rino *et al.* 2008). Palaeotectonic reconstructions are key to our understanding of these interrelated processes and constrain the timing, duration and style of magmatism. The construction of Gondwana was a protracted and complex process whereby microcontinents, such as Avalonia, were amalgamated onto, and incorporated within, the emerging land mass (Cawood *et al.* 2021). The Neoproterozoic of southern Britain represents a prolonged (*c.* 200 Ma) period of discontinuous magmatism, which necessitates accurate age-constrained isotopic and geochemical signatures to reconstruct the tectonic setting of peri-Gondwanan terranes in this area (Pharaoh and Carney 2000; Compston *et al.* 2002; Schofield *et al.* 2016).

Drill core and geophysical data indicate that England and Wales (south of the Iapetus suture) are underlain by a mosaic of Avalonian terranes, which, from west to east, include the Cymru, Wrekin, Charnwood and Fenland terranes (Pharaoh and Carney 2000; McIlroy and Horak 2006; Schofield *et al.* 2016). However, complications arise from the sparsely distributed, fault-uplifted tectonic inliers (Fig. 1) and the varying degrees of deformation and metamorphism sustained by the Precambrian basement lithologies during the Caledonian, Variscan and Alpine orogenies (Pharaoh and Carney 2000). The Johnston Complex, the Arfon and Sarn groups of North Wales and the Pebidian Supergroup of north Pembrokeshire have been assigned to the Cymru Terrane (Pharaoh and Carney 2000; Schofield *et al.* 2016) (Fig. 1). However, other workers have questioned the reliability of such broad terrane associations based on limited basement outcrops and the internal complexities of individual inliers (Compston *et al.* 2002; Schofield *et al.* 2016). The Johnston Complex typifies this issue; based on published zircon U–Pb ages and its calc-alkaline geochemistry, it has been classified into either the Wrekin Terrane (McIlroy and Horak 2006) or the Cymru Terrane (Fig. 1) (Pharaoh and Carney 2000; Compston *et al.* 2002; Schofield *et al.* 2016). East Avalonian terranes are interpreted to represent remnants of a single late Neoproterozoic subduction margin (Pharaoh *et al.* 1987). As such, constraining the tectonomagmatic processes during this formative period in the evolution of Earth systems relies on accurate terrane designations, which, in turn, underpin palaeocontinental reconstructions, essential to constraining the relationships between different planetary geochemical reservoirs during important intervals in Earth history (Fig. 1) (Strachan *et al.* 2007; Nance *et al.* 2008).

As there is a general paucity of recent isotopic studies, previous terrane classification work has relied on sparse isotopic and geochemical data (Fig. 1) (Pharaoh and Carney 2000; Schofield *et al.* 2016). The Johnston Complex of SW Wales is a case in point, with research into the Johnston Complex being limited to Cantrill *et al.* (1916), Thorpe (1972) and the isotopic analyses of Patchett and Jocelyn (1979) and Schofield *et al.* (2016). Despite representing some of the oldest rocks in southern Britain, with a reported zircon U–Pb age of 643 +5/−28 Ma (Patchett and Jocelyn 1979), few other isotopic data are available for the Johnston Complex, aside from a whole-rock Nd analysis undertaken by Schofield *et al.* (2016). Hence the context of the Johnston Complex within the broader peri-Gondwanan magmatic realm is yet to be fully determined. Several details remain unresolved, including the degree of heterogeneity within the Johnston Complex (single pluton v. composite magmatic body), the character of its source

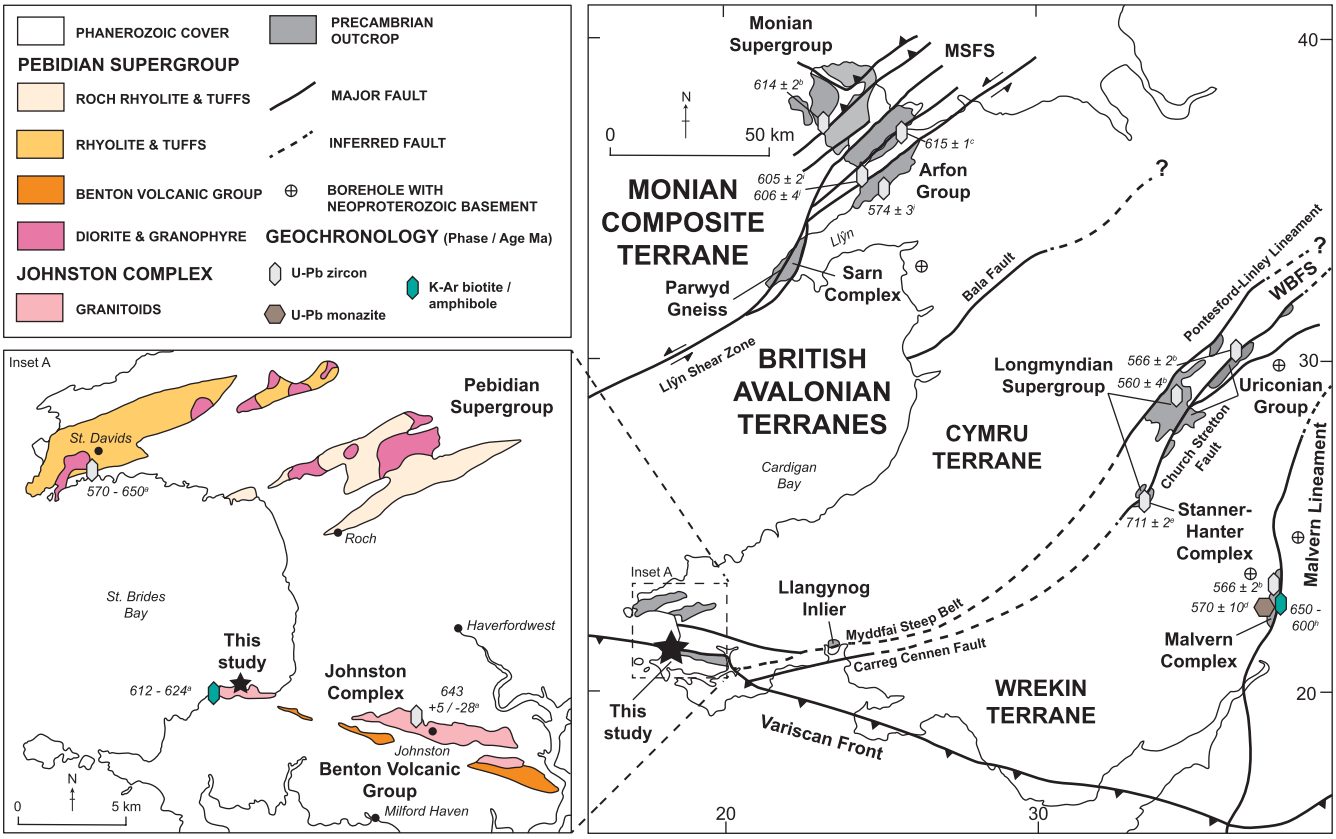

Fig. 1. Distribution of Precambrian outcrops in southern Britain. Previous ages obtained from the Johnston Complex include Patchett and Jocelyn (1979) and unpublished K–Ar ages for muscovite and hornblende discussed by Patchett and Jocelyn (1979). The coordinate system used is the UK National Grid. WBFS, Welsh Borderland Fault System; MSFS, Menai Strait Fault System. Data sources are identified by superscript letters: [a] Patchett and Jocelyn (1979), [b] Tucker and Pharaoh (1991), [c] Horak *et al.* (1996), [d]Thorpe *et al.* (1984), [e] Schofield *et al.* (2010), [f] Noble *et al.* (1993), [g] Beckinsale *et al.* (1984), [h] Strachan *et al.* (1996) and [i] Compston *et al.* (2002). Schematic tectonic map of southern Britain adapted after Pharaoh and Carney (2000); inset map of Precambrian geology in Pembrokeshire modified after Bloxam and Dirk (1988).

rocks, the relationship of the complex to the surrounding inliers and its ultimate terrane classification.

This paper presents *in situ* zircon (U–Pb, Lu–Hf), apatite (U–Pb) and trace element data from the Johnston Complex for both minerals. Our results demonstrate that the complex is a composite magmatic body composed of discrete quartz diorite plutons along its *c.* 20 km length. Our data show that calc-alkaline magmatism persisted in an ensialic setting in East Avalonia to *c.* 570 Ma, prior to oblique convergence and terrane dispersal. We demonstrate that the source melt of the Johnston Complex was derived from a uniform and broadly chondritic source from 615 to 570 Ma, consistent with evolved εNd values from East Avalonia. The chemical data presented here reinforce the classification of the Johnston Complex within the Cymru Terrane of East Avalonia and show an S-type component within the melt. We demonstrate that a combined apatite and zircon geochronology approach constrains inherited v. primary zircon within S-type granitoids and clarifies the post-magmatic history of an igneous body.

Geological background

Regional geology

The Menai Strait Fault separates the Precambrian geology of southern Britain into the Avalonian and Monian tectonic blocks (Fig. 1) (Strachan *et al.* 2007; Woodcock *et al.* 2012; Schofield *et al.* 2016). Several terranes within these blocks (e.g. the Cymru, Charnwood, Fenland and Wrekin terranes) comprise the Avalon Composite Terrane, which is primarily concealed by Phanerozoic rocks (Pharaoh and Carney 2000; Schofield *et al.* 2016). Major fault zones, such as the Malvern fault system and the Welsh Borderland fault system, represent the broad structural controls on the distribution of Neoproterozoic inliers in southern Britain (Fig. 1) (Pharaoh and Carney 2000; Woodcock *et al.* 2012). The ultimate relationship between the Avalonian and Monian terranes remains unresolved. However, both share a history of calc-alkaline magmatism, accretionary prism and basement gneiss amalgamation during the late Neoproterozoic (Woodcock *et al.* 2012; Schofield *et al.* 2016). Isotopic and structural data point towards a shared genesis for both units (Horak *et al.* 1996) and, taken together, they are termed the Avalon Superterrrane.

Geology of the Johnston Complex

The Precambrian rocks of SW Wales crop out in two areas north and south of St Brides Bay (Fig. 1). To the south is the Johnston Complex, an east–west-trending intrusive suite of felsic plutons consisting of diorites, tonalites and granodiorites (Thorpe 1972). These rocks are cross-cut by metre-scale dolerite dykes emplaced during the Variscan Orogeny (Thorpe 1972, 1979; Patchett and Jocelyn 1979). The Johnston Complex is exposed in two outcrops: a coastal section on the southern end of St Brides Bay and an inland area within the Bolton Hill Quarry near the eponymous town of Johnston (Fig. 1). The Johnston Complex is thrust on top of Paleozoic sedimentary rocks and is entrained within the hanging wall of the Johnston–Benton thrust zone (Woodcock *et al.* 2012). The coastal outcrop of the Johnston Complex consists of quartz diorite, which is dominated by plagioclase (oligoclase to andesine), quartz, partially altered primary mafic minerals (hornblende and

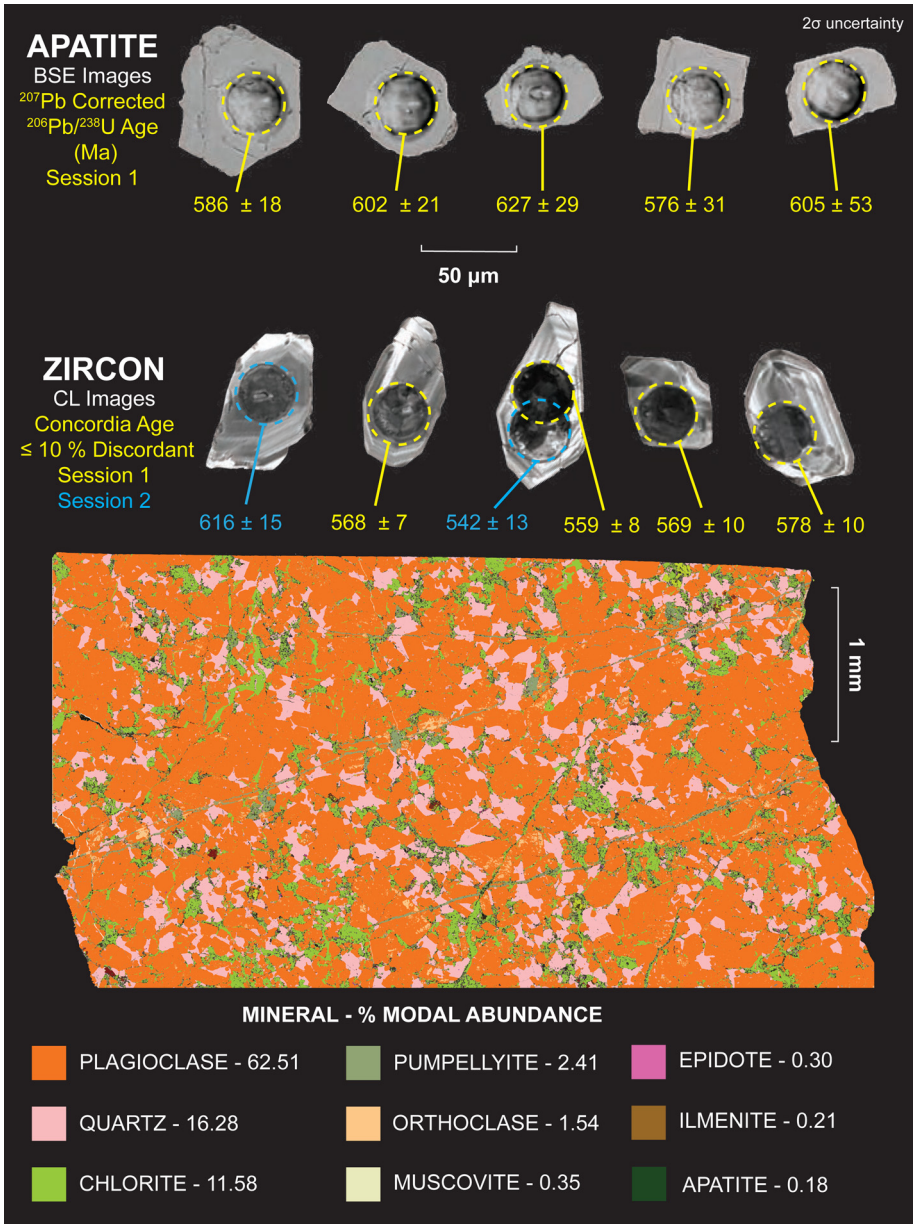

Fig. 2. Top row: Back-scattered electron images of representative apatite showing 38 µm spots and the F207 corrected age. Second row: cathodoluminescence images of zircon showing the concordia ages and the 38 µm spot obtained from separate sessions. Third row: Tescan Integrated Mineral Analyser phase map of minerals with a mass percentage >0.10 for the quartz diorite of the Johnston Complex.

biotite) now occurring as chlorite, sericite and illite, and minor iron–titanium oxides (Fig. 2).

There is some lithological variability between the inland portion and coastal outcrops. The inland lithologies have an increased abundance of hornblende and biotite, but alkali feldspar is mainly absent (Thorpe 1972, 1979). By contrast, the coastal outcrops have a more homogenous quartz diorite composition and contain orthoclase at <2% modal abundance (Thorpe 1972).

Methods

Mineral separation

A sample of quartz dolerite from the Johnston Complex was collected from south of St Brides Bay (51° 46′ 21.6′ N, 5° 08′ 57.1′ W). Zircon and apatite grains were separated following standard procedures at the John De Laeter Centre (JdLC), Curtin University, Perth, Australia. The sample was crushed using a ring mill and sieved to yield the ≤425 µm fraction. This fraction underwent heavy mineral separation via a Jasper Canyon Research water-shaking table (Dumitru 2016). Lithium heteropolytungstate heavy liquid separation at 2.85 g cm^{-3} and Frantz isodynamic separation followed to produce a final fraction that was mounted in entirety onto a 25 mm epoxy resin round.

A polished 4 cm × 2 cm block was also prepared and analysed via a Tescan Integrated Mineral Analyser (TIMA) to provide insights into texture and mineralogy. Both the round mount and block were polished using a 1 µm diamond suspension fluid and imaged using reflected and transmitted light. TIMA analysis was used to identify mineral phases on the mount and block and a Clara field-emission scanning electron microscope was then used to provide high-resolution images of the internal grain morphology, aiding spot placement during laser ablation inductively coupled plasma mass spectrometry (LA-ICP-MS).

Isotopic analyses

Zircon U–Pb and Lu–Hf geochronology

A single session of split-stream zircon U–Pb and Lu–Hf analysis was undertaken at the GeoHistory Facility at the JdLC. A RESOlution LE193 nm ArF laser and a Lauren Technic S155 cell were used to ablate the zircon and an Agilent 8900 inductively coupled plasma mass spectrometer was used to collect U–Pb data. The Lu–Hf isotopes were collected simultaneously via a Nu Plasma

II multi-collector inductively coupled plasma mass spectrometer. The relatively small grain size of zircon (typically <70 μm in length) and internal complexities necessitated a comparatively small spot size of *c.* 38 μm diameter.

The matrix-matched primary reference material used for zircon U–Pb data reduction was GJ1 (Jackson *et al.* 2004). The Plešovice (337.13 ± 0.37 Ma) (Sláma *et al.* 2008) and 91500 (1063.78 ± 0.65 Ma) (Wiedenbeck *et al.* 1995) secondary reference materials were used to monitor the accuracy of the $^{238}U/^{206}Pb$ ratio measurement. To check the accuracy of the $^{207}Pb/^{206}Pb$ ages, OG1 (3465.4 ± 0.6 Ma) (Stern *et al.* 2009) was reduced against Maniitsoq (3008.70 ± 0.72 Ma) (Marsh *et al.* 2019). All the weighted mean ages for the secondary reference materials were within 2σ uncertainty of the accepted values (Appendix 1, Supplementary Material).

Mud Tank zircon (Woodhead *et al.* 2004) was the primary reference material for the zircon Lu–Hf analyses. Several secondary reference zircons, including GJ1 (0.282000 ± 0.000025) (Morel *et al.* 2008), 91500 (0.282306 ± 0.00004) (Woodhead *et al.* 2004; Woodhead and Hergt 2005) and R33 (0.282764 ± 0.000014) (Fisher *et al.* 2014*a*) were measured to confirm the accuracy. All the reference materials gave $^{176}Hf/^{177}Hf$ ratios within 2σ uncertainty of the accepted values and the stable $^{178}Hf/^{177}Hf$ ratio was also within 2σ uncertainty of the expected ratio (Appendix 1, Supplementary Material) (Sláma *et al.* 2008; Fisher *et al.* 2014*b*).

Apatite U–Pb

Two sessions of apatite U–Pb isotopic analyses were completed at the GeoHistory Facility, JdLC, using a RESOlution 193 nm ArF laser with a Lauren Technic S155 cell and an Agilent 8900 inductively coupled plasma mass spectrometer. Given the small grain size (<50 μm) of apatite from the Johnston Complex, a 38 μm spot size was ablated using a 5 Hz repetition rate and a fluence of *c.* 2 J cm^{-2}. Madagascar (MAD-2) (Thompson *et al.* 2016) and Mt McClure (MMC) (Schoene and Bowring 2006) apatite were used as the primary reference material for sessions 1 and 2, respectively. The secondary reference material analysed included the MMC apatite (523.51 ± 1.47 Ma), the Duluth Complex (FC) apatite (1099.1 ± 0.2 Ma) (Schmitz *et al.* 2003) and the Durango apatite (31.44 ± 0.18 Ma) (McDowell *et al.* 2005). The ages obtained via unanchored regressions through the secondary reference apatite were within 2σ uncertainty of accepted ages (Appendix 2, Supplementary Material).

Apatite and zircon trace elements

A single session of zircon and apatite trace element analysis was performed at the GeoHistory Facility at the JdLC. *In situ* trace element measurements were made on some grains not previously analysed during earlier U–Pb sessions using an Agilent 8900 inductively coupled plasma mass spectrometer. The size of the zircon and apatite grains necessitated a 38 μm spot size at a fluence of 2.5 J cm^{-2} and a 5 Hz laser pulse rate.

NIST 610 was used as the primary reference material for zircon analyses to calculate elemental abundance and correct for instrumental drift. The internal reference isotope used was ^{29}Si, assuming a stoichiometric zircon composition of 14.76 wt% silicon. Secondary reference materials included 91500 zircon, using the reported values of Sano *et al.* (2002), and NIST 612 (Jochum *et al.* 2005). For both reference materials, the measured abundances were within 5–10% of the reported values.

NIST 610 was the primary reference material for apatite trace element analyses. ^{29}Si was used as the internal reference isotope, assuming an apatite Si content of 0.41 wt% (Azadbakht *et al.* 2018). Secondary reference materials included the Durango apatite and NIST 621 glass; the measured abundances were generally within 10% of the reported values (Jochum *et al.* 2005; McDowell *et al.* 2005).

Results

Petrography

The results of the automated mineralogy undertaken via TIMA are consistent with the previous petrographic accounts of Cantrill *et al.* (1916) and Thorpe (1972). The Johnston Complex sample is a mesocratic medium-grained (1–5 mm) quartz diorite to tonalite principally composed of plagioclase feldspar (oligoclase to andesine) and quartz (Fig. 2). The primary mafic minerals (hornblende and biotite) are variably altered to hydrous secondary phases, including chlorite, sericite and illite. Accessory minerals within this rock include apatite, zircon, muscovite and iron–titanium oxides, including rutile and hematite (Fig. 2). Orthoclase occurs at low modal abundances (<2%) within antiperthite textures. Veinlets of pumpellyite cross-cut the sample (Fig. 2), consistent with the low-grade of metamorphism experienced by the Johnston Complex and other Neoproterozoic inliers in SW Wales (Thorpe 1972; Patchett and Jocelyn 1979). There is a general lack of significant metamorphic and deformational overprint in the sample, with only limited strained quartz, consistent with the rock fabric being dominantly magmatic.

Zircon

Zircon morphology

Zircon grains from the Johnston Complex are colourless to light brown, tabular, euhedral to subhedral and are mainly intact crystals. Pristine grains have aspect ratios of ≥3:1. The grain size is variable, but does not typically exceed 200 μm in length. Sharp oscillatory zoning, with well-defined core–rim relationships (based on the cathodoluminescence response), is apparent in the zircon population. Small anhedral ≤10 μm apatite inclusions are found within some zircon crystals.

The zircon grains are predominantly situated on the margins of quartz or are contained within plagioclase and quartz (Fig. 3a, b). Zircon is also associated with altered hydrous phases such as chlorite (Fig. 3a). A petrographic relationship between zircon and mafic minerals has been observed in many granitoids and attributed to enhanced local Zr saturation (Bacon 1989; Elburg 1996) or greater zircon growth potential in localized volatile-rich melt pockets (Miller *et al.* 2007; Erdmann *et al.* 2013). Zircon is absent in the late pumpellyite veinlets (Fig. 3a).

Zircon U–Pb and Lu–Hf geochronology and trace element chemistry

Over two analytical sessions, 124 U–Pb isotopic analyses were performed on zircon grains, from which 29 were <10% discordant. In the Tera–Wasserburg plot, some zircon analyses scatter towards lower $^{238}U/^{206}Pb$ ratios at constant $^{207}Pb/^{206}Pb$, interpreted to reflect recent radiogenic Pb loss (Fig. 4).

The concordant analyses define two coherent groups of ages (populations 1 and 2). Group 1 yields a concordia age of 569 ± 2 Ma [n = 27, MSWD = 1.9, $p(x^2)$ = 0.079], which is interpreted as the magmatic crystallization age for the quartz diorite, consistent with the oscillatory zoned zircon textures for this component (Fig. 2).

Population 2 is defined by two zircon core analyses and is statistically distinct from population 1, yielding an older concordia age of 615 ± 11 Ma [MSWD = 0.28, $p(x^2)$ = 0.89]. Population 2 is interpreted to represent older cores and was exclusively collected from larger zircon grains, which allowed individual cores to be analysed (Fig. 2). Given the low number of analyses, these grains

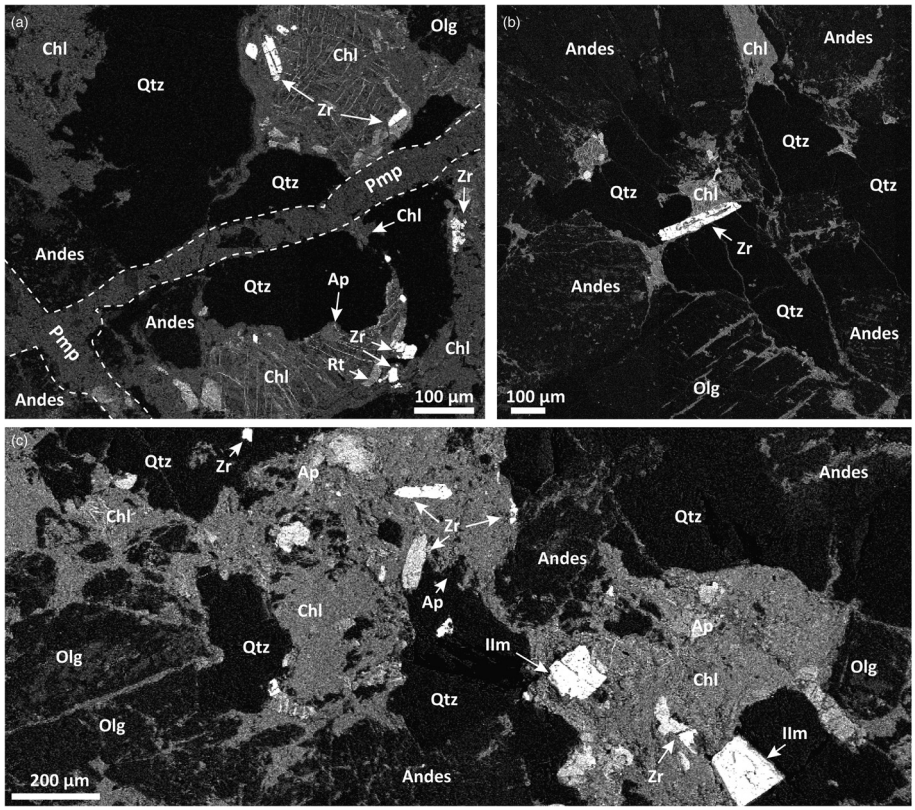

Fig. 3. Compilation of representative back-scattered electron images showing zircon and apatite mineral associations. Andes, andesine; Ap, apatite; Chl, chlorite; Ilm, ilmenite; Olg, oligoclase; Pmp, pumpellytite; Qtz, quartz; Rt, rutile; Zr, zircon.

could represent either rare inherited zircons assimilated from the wall rock or an antecrystic component from an earlier magmatic episode within the same longer-lived igneous system. The similarity of the zircon rare earth elements (REEs) and the Lu–Hf chemistry between populations 1 and 2 supports the latter interpretation.

Zircon REE chondrite-normalized (Boynton 1984) plots show positively sloping gradients with cerium enrichment and europium depletion (Fig. 5). The mean cerium anomaly (Ce/Ce*) for zircon from the Johnston Complex is +1.48, whereas the Eu anomaly $(Eu/Eu^*)_{CN}$ is strongly negative at 0.28. Some analyses show flattening of the light REE (LREE) v. medium REE (MREE) slope [LREE/MREE, $(La/Sm)_{CN}$], consistent with a gain of non-stoichiometric elements into metamict zircon. These analyses typically yield discordant U–Pb isotopic results (Fig. 4).

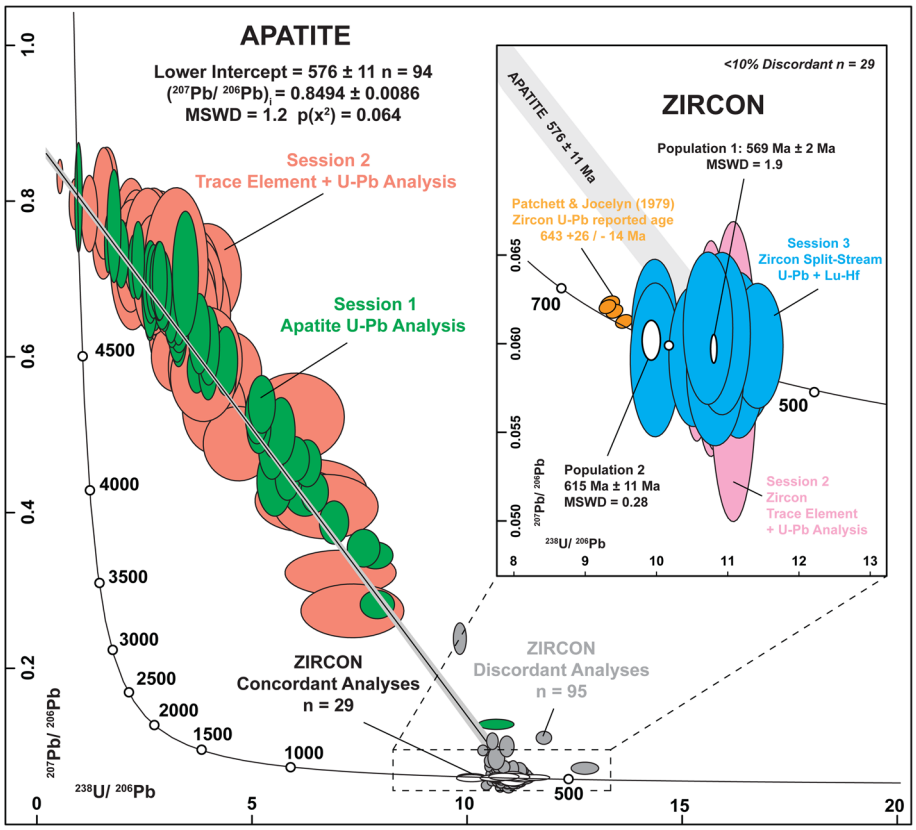

Fig. 4. Tera–Wasserburg plot for zircon and apatite of the Johnston Complex. Note the different precisions of U–Pb analyses across each session, a function of the LA-ICP-MS counting time during U–Pb analyses, and trace element analysis compared to split-stream U–Pb and Lu–Hf. The inset shows the lower intercept of the apatite U–Pb regression, a magnified view of zircon U–Pb analyses and the earlier thermal ionization mass spectrometry results of Patchett and Jocelyn (1979).

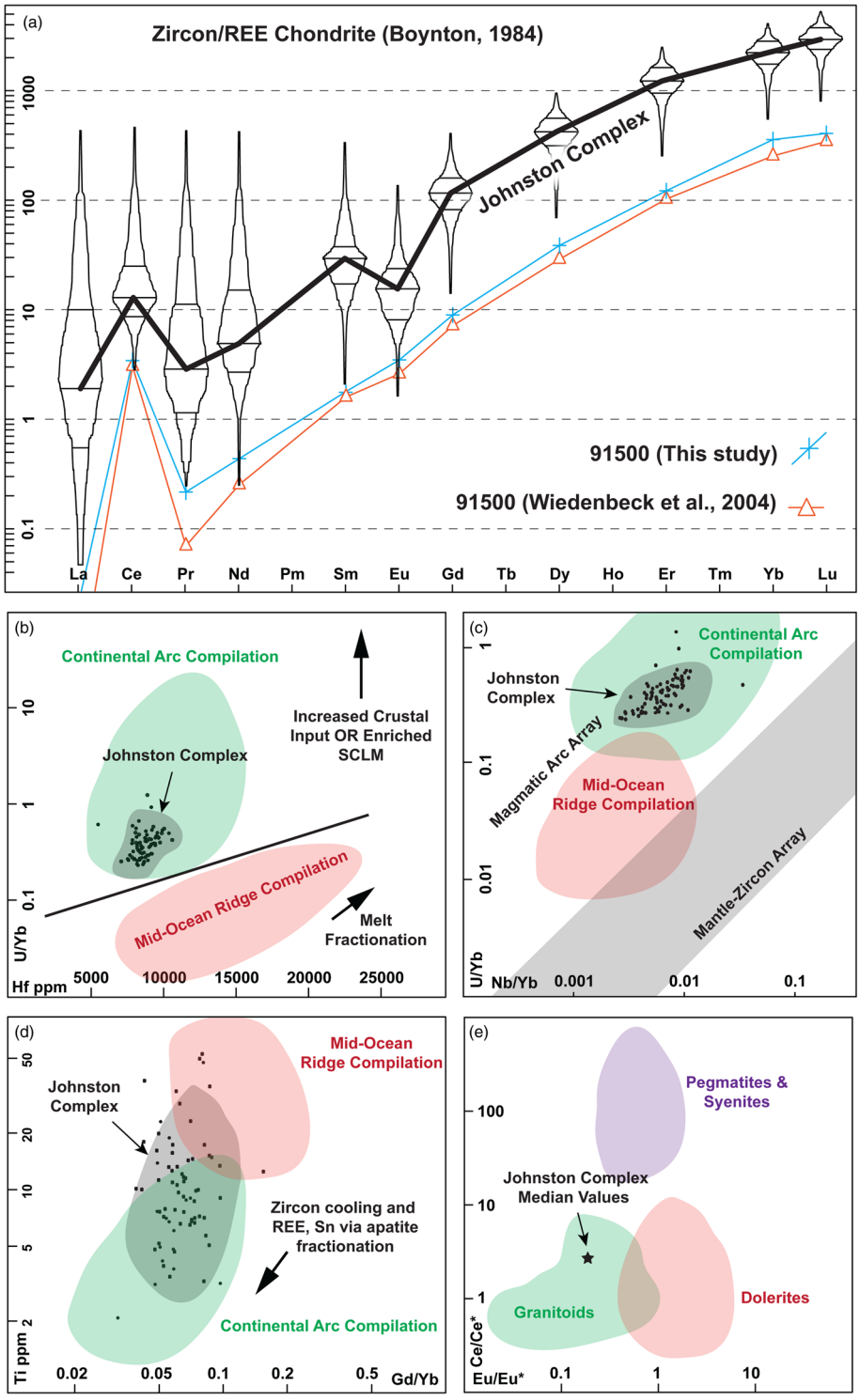

Fig. 5. Zircon geochemistry discrimination diagrams. (**a**) REE chondrite-normalized zircon multi-element plot (after Boynton 1984). (**b–d**) Bivariate plots of zircon geochemistry with compositional reference fields after Grimes *et al.* (2015). (**e**) Eu/Eu* v. Ce/Ce* anomalies. Compositional reference fields adapted from Belousova *et al.* (2002*a*). SCLM, subcontinental lithospheric mantle.

A total of 44 zircon Lu–Hf analyses were obtained (Fig. 6). Analyses of concordant zircon yield an εHf of −4.0 to 2.9 for population 1 with a weighted mean of −0.41 ± 1.38 (MSWD = 0.68). The population 2 εHf values range from −4.0 to −1.2 (Fig. 6). Both populations yield similar model ages with a mean Lu–Hf T^2_{DM} of 1521 Ma.

Apatite

Apatite morphology

Apatite from the Johnston Complex typically occurs as small (*c.* 50 μm) (Fig. 3) subhedral equant grains, although the largest euhedral apatite is >120 μm long. Most grains are intact with hexagonal basal sections. Apatite grains are largely colourless to light brown and internally homogenous without inclusions. Apatite is primarily associated with hydrous minerals (i.e. chlorite) and some grains occur within quartz, oligoclase and andesine (Fig. 3).

Apatite U–Pb geochronology

A total of 94 apatite U–Pb analyses define a discordant array on the Tera–Wasserburg concordia diagram, spanning between a $^{207}Pb/^{206}Pb$ value of 0.85 ± 0.0086 at the upper intercept to an apparent age of 576 ± 11 Ma at the radiogenic lower intercept [MSWD = 1.2; $p(x^2)$ = 0.064]. The F207% of the apatite analyses ranges from 12 to 99% with a mean value of 69% (Fig. 4). F207% defines the distance along a mixing line between the non-radiogenic (common Pb) and radiogenic

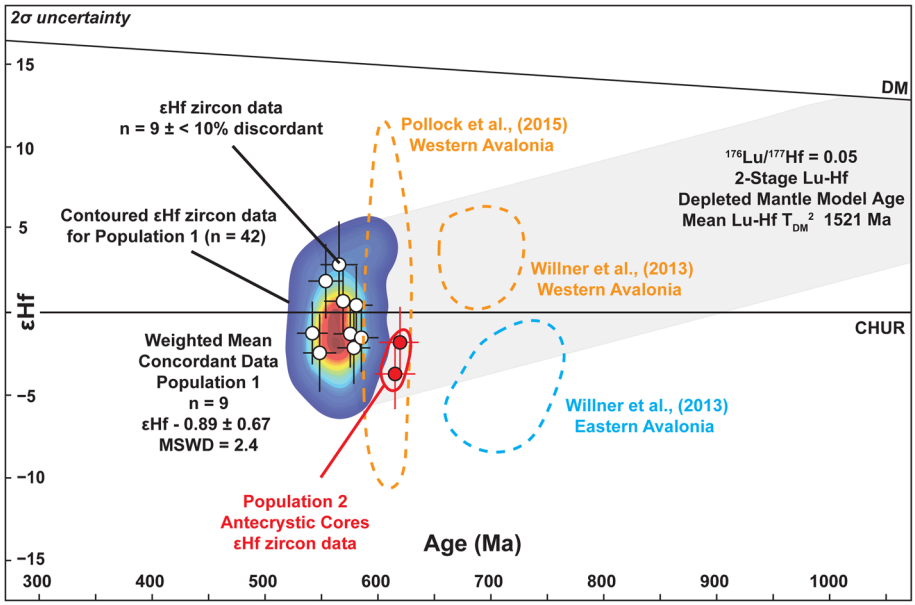

Fig. 6. εHf plot for zircon of the Johnston Complex and other Avalonian terranes. Data contoured using a kernel bandwidth of 10 for the *x*-axis and 1.25 intervals for the *y*-axis. εHf data compiled from Pollock *et al.* (2015) and Willner *et al.* (2013). CHUR, chondritic uniform reservoir; DM, depleted mantle.

Pb components, where a higher percentage implies a greater common Pb component (Kirkland *et al.* 2017).

Apatite trace element chemistry

The uranium concentration of the apatite ranges from 1.3 to 151.6 ppm and the mean concentration is 9.2 ppm. Thorium concentrations range from 2.9 to 203.5 ppm with a mean value of 25.8 ppm. The REE chondrite-normalized plots (Boynton 1984) show a characteristic negative slope from light to heavy REEs, with a median $(La/Sm)_{CN}$ value of 2.6. The europium anomaly (Eu/Eu*) of the apatite is comparable with that in zircon at 0.35 (Fig. 7).

Discussion

The Johnston Complex: a composite magmatic body

The ages yielded by the population 1 zircon and apatite analyses are identical within uncertainty and yield a combined weighted mean age of 570 ± 3 Ma (MSWD = 1.5) (Fig. 4), interpreted as the crystallization age of the quartz diorite component of the Johnston Complex. This *c.* 570 Ma age contrasts with the only previously reported U–Pb age for the Johnston Complex of 643 +5/−28 Ma (Patchett and Jocelyn 1979) (Fig. 1). Previous workers, including Patchett and Jocelyn (1979) and Thorpe (1979), concluded that the entire Johnston Complex (aside from the dolerite dykes) was emplaced at *c.* 643 Ma. Assuming that the multi-grain zircon fractions reported by Patchett and Jocelyn (1979) reflect a magmatic event, the apparent *c.* 643 Ma U–Pb age implies an earlier stage of magmatism for an inland component of the Johnston Complex. This interpretation is consistent with the observation that different multi-grain size fractions of the Patchett and Jocelyn (1979) dataset define a single lower intercept with no excess dispersion (Fig. 4). Here, we also report an older ≥615 Ma antecrystic zircon core component (population 2) within the coastal outcrop of the Johnston Complex (Fig. 4).

We analysed a sample collected 9 km to the west of the study site of Patchett and Jocelyn (1979). Geophysical data and field observations show that both outcrops of the Johnston Complex are bound within the Johnston–Benton thrust zone and share a quartz diorite composition (Thorpe 1979; Woodcock *et al.* 2012). Our isotopic data therefore indicate that the Johnston Complex represents discrete magmatic units with ages spanning over 40 Ma (Fig. 4). Hence previous accounts that the Johnston Complex represented a single magmatic episode at *c.* 650 Ma (Pharaoh and Carney 2000; Woodcock *et al.* 2012; Valley *et al.* 2014) now appear inconsistent with the younger Cryogenian history of plutonism recorded within the apatite and zircon of the western Johnston Complex.

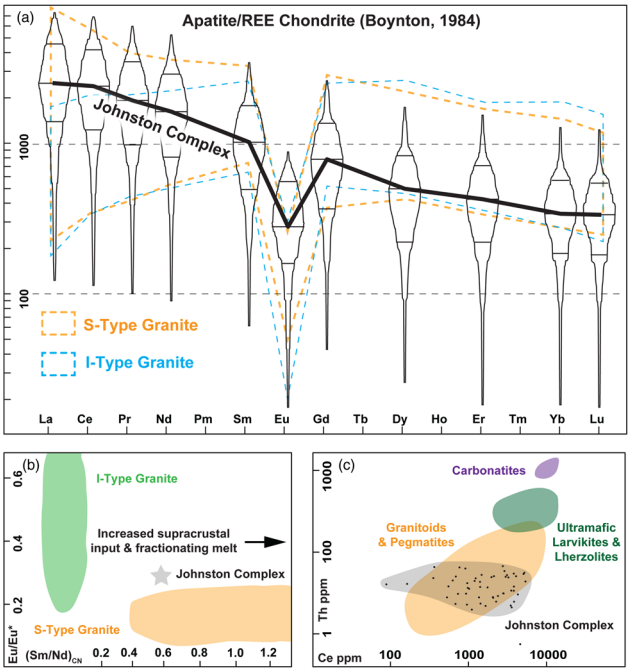

Fig. 7. Apatite geochemistry discrimination diagrams. (**a**) REE chondrite-normalized apatite multi-element plot (Boynton 1984). Compositional data for granitoids from O'Sullivan *et al.* (2020). (**b**) Bivariate plot of the mean europium anomaly $(Eu/Eu^*)_c$ v. chondrite-normalized Sm/Nd_c. Contoured compositional fields after Sha and Chappell (1999). (**c**) Bivariate plot of apatite Th v. Ce abundance. Compositional reference fields adapted after Belousova *et al.* (2002*b*).

Neoproterozoic igneous activity in southern Britain has been summarized via a three-stage model (Pharaoh and Carney 2000; Woodcock *et al.* 2012). Based on the new geochronology reported herein, the Johnston Complex retains information from each stage (Fig. 8). An early *c.* 700–640 Ma period of magmatism is recorded throughout the basement of southern Britain and is characterized by pluton emplacement at mid-crustal depths within the Wrekin Terrane – for example, the Stanner–Hanter Complex and the

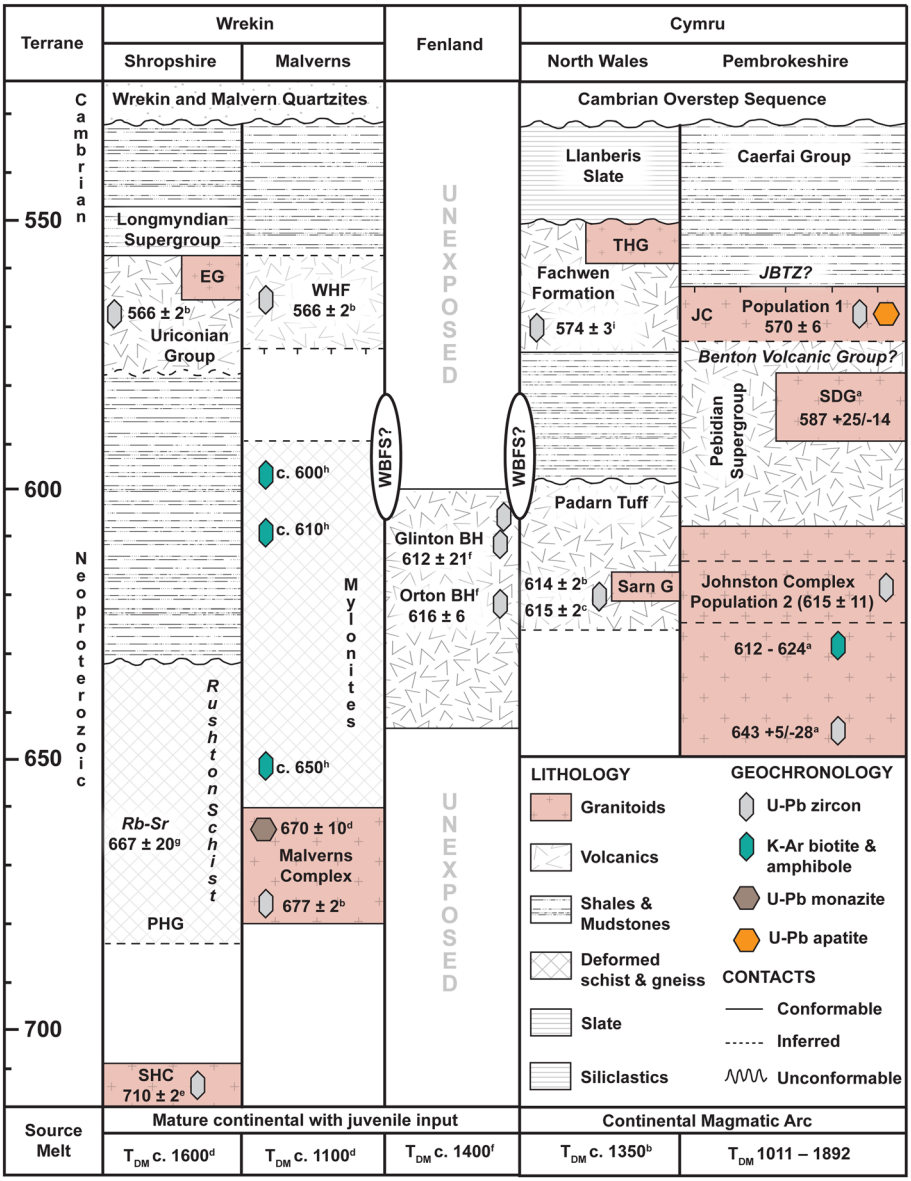

Fig. 8. Stratigraphic terrane correlation chart of selected areas. Data sources are listed as superscript letters: [a] Patchett and Jocelyn (1979), [b] Tucker and Pharaoh (1991), [c] Horak *et al.* (1996), [d] Thorpe *et al.* (1984), [e] Schofield *et al.* (2010), [f] Noble *et al.* (1993), [g] Beckinsale *et al.* (1984), [h] Strachan *et al.* (1996) and [i] Compston *et al.* (2002). BH, borehole data; EG, Ercall granophyre; JBTZ, Johnston Benton thrust zone; JC, Johnston Complex; SDG, St David's granophyre; SHC, Stanner–Hanter Complex; THG, Twt Hill Group; WBFS, Welsh Borderland Fault System. Figure adapted after Pharaoh and Carney (2000).

Malverns (Fig. 1) (Pharaoh and Carney 2000). The inland *c.* 643 Ma pluton of the Johnston Complex (Patchett and Jocelyn 1979) thus brackets the end of this earliest stage of magmatism.

Calc-alkaline arc plutons (the Sarn Complex, Arfon Group) and volcanic sequences (the Pebidian Supergroup) dominated a later period of magmatism from *c.* 620 to 585 Ma during the so-called Main Magmatic Event within the British Avalonian terranes (Pharaoh and Carney 2000). The *c.* 615 Ma zircon core age and *c.* 570 Ma zircon and apatite U–Pb age (Fig. 4) constrain the age of the western portion of the Johnston Complex to a hitherto unidentified younger expression of the Main Magmatic Event. The *c.* 615 Ma zircon core age is coeval with a 614 ± 2 Ma age reported for the Arfon Group (Fig. 8) (Tucker and Pharaoh 1991), indicating an interval of calc-alkaline plutonism in the Cymru Terrane at this time (Schofield *et al.* 2016). Furthermore, zircon U–Pb data from the Fenland Terrane also record magmatism at 615 ± 6 Ma (Noble *et al.* 1993). Based on the shared *c.* 615 Ma age and εNd signatures, Schofield *et al.* (2016) posited that the Fenland Terrane, Arfon Group and Sarn Complex were the disrupted remains of a single basement unit. The context of the Johnston Complex to this purported basement block remains enigmatic as we report only two *c.* 615 Ma grain cores; nonetheless, it is noteworthy that magmatism of this age has not been documented from the Cymru, Wrekin and Charnwood terranes (Schofield *et al.* 2016).

Despite their close geographical proximity (Fig. 1), the relationship between the Pebidian Group and Johnston Complex remains unresolved and this has led to these two inliers having variable terrane classifications; see McIlroy and Horak (2006) cf. Pharaoh and Carney (2000). A minimum age of *c.* 587+25/−14 Ma is reported for the Pebidian Group from the cross-cutting St David's granophyre (Patchett and Jocelyn 1979). The *c.* 570 Ma age obtained from zircon and apatite in this study, combined with the strongly calc-alkaline affinities of both inliers, points towards a genetic relationship between the Pebidian Supergroup and Johnston Complex, thereby supporting the position of the Johnston Complex within the Cymru Terrane. If so, the coastal pluton of the Johnston Complex would be constrained to the final stage of magmatism, defined by the transition from a magmatic-dominated regime to one of sedimentation and oblique terrane dispersal (Pharaoh and Carney 2000; Woodcock *et al.* 2012).

McIlroy and Horak (2006) posited that the Welsh Borderland fault system (Fig. 1) represented a terrane boundary between the Wrekin and Cymru terranes. The combined *c.* 570 Ma apatite and zircon magmatic crystallization age and their continental arc geochemical signatures support the association of the Johnston Complex with the Cymru Terrane. Northern constituents of the Cymru Terrane (e.g. the Arfon Group and Sarn Complex) share a geochemical affinity with the Pebidian Supergroup and Johnston

Complex. To the east, the undated Coomb Volcanic Formation differs significantly and has intra-continental bimodal geochemical signatures (Fig. 1) (Bevins *et al.* 1995). Other components of the Wrekin Terrane, such as the Longmyndian and Uriconian groups, also share a pronounced intra-plate geochemistry, suggesting a decreasing influence of subduction-related magmatism towards the east (McIlroy and Horak 2006). We therefore suggest that the eastern margin of the Johnston Complex, the inferred extension of the Carreg Cennen Fault, is a terrane boundary separating the Cymru and Wrekin terranes (Fig. 1).

The relationship between the Benton Volcanic Group and the Johnston Complex is uncertain (Fig. 1). Nonetheless, the entrainment of both inliers within the Johnston–Benton thrust zone and their shared calc-alkaline chemistry (Thorpe 1972; Bevins *et al.* 1995) implies a common magmatic source for both units. The rhyolitic lavas and tuffs of the Benton Group are posited to represent more evolved expressions of eruptives in the Pebidian Supergroup to the north (Baker 1982; Bevins *et al.* 1995). Given the potential linkage between the Pebidian Supergroup and the Johnston Complex, the Benton Group warrants further analysis to determine its broader terrane affinity and relationship to the Johnston Complex. The Johnston Complex now provides constraints on the evolution of the Cymru Terrane itself, representing some of the oldest (*c.* 640 Ma) (Patchett and Jocelyn 1979) and youngest (*c.* 615–570 Ma) magmatism in the area.

Geochemistry of the Johnston Complex

Zircon geochemistry: continental magmatic arc affinities

Previous accounts of the geochemistry of the Cymru Terrane (Thorpe 1972; Pharaoh *et al.* 1987; Bevins *et al.* 1995) have reported calc-alkaline geochemical signatures consistent with subduction-related continental arc magmatism. Our new zircon and apatite data reinforce these earlier interpretations and provide insights into the geochemistry of the late Main Stage magmatism in the Cymru Terrane. The chondrite-normalized (Boynton 1984) REE plots for zircon from the Johnston Complex show positively sloping trends with Ce and Sm enrichment and Pr and Eu depletion (Fig. 5). Oxidized Ce^{4+} is more compatible with zircon than the more reduced cations of cerium (Belousova *et al.* 2002*a*). Accordingly, the positive cerium anomaly (+1.48, Fig. 5) is a broad reflection of the oxidized nature of the source magma for the Johnston Complex (Belousova *et al.* 2002*a*). Subduction-derived melts are typically oxidized, with the zircon Ce enrichment of the Johnston Complex analogous to the modern Indonesian subduction system (Woodcock *et al.* 2012; Bénard *et al.* 2018).

Zircon crystals derived from fractionated granitoid melts generally show a negative Eu anomaly, representing Eu^{2+} sequestration during oligoclase and andesine crystallization. The zircon Eu anomaly reported here (0.28) is consistent with an evolved source melt and the high abundance of plagioclase within the quartz diorite of the Johnston Complex (Fig. 2) (Appendix 1, Supplementary Material).

The geochemical data suggest that evolved calc-alkaline plutonism persisted in the Cymru Terrane to at least *c.* 570 Ma and the emplacement of the Johnston Complex was therefore contemporaneous with the terrane dispersal and oblique convergence associated with the final stage of Neoproterozoic magmatism in southern Britain (Pharaoh and Carney 2000). The geochemical profiles of the Johnston Complex and the Pebidian Supergroup represent an archive of the evolving tectonic setting of the Cymru Terrane from a time of mid-crustal plutonism at *c.* 640–615 Ma (Johnston Complex) to intercalated volcanism and sedimentation within the Welsh Basin during the Paleozoic (Pebidian Supergroup). Late Neoproterozoic <580 Ma components of the Wrekin Terrane, such as the Uriconian and Warren House groups, have geochemical affinities that shifted towards more intra-plate bimodal components. Such geochemical trends point towards later arc rifting, suggesting a more distal location from the subducting front for these units (Bevins *et al.* 1995; Pharaoh and Carney 2000). Our geochemical data (Fig. 5) are consistent with the Johnston Complex retaining a uniform evolved calc-alkaline magmatic signature from *c.* 640 to 570 Ma, suggesting a lack of source magma modification prior to terrane dispersal after *c.* 570 Ma.

Apatite geochemistry: Gondwanan S-type granite production

Unlike the zircon from the Johnston Complex, the apatites do not show a pronounced cerium anomaly (Ce/Ce* = 0.02) (Fig. 7). Such a trend is typical of evolved felsic melts, where cerium is sequestered into fractionating plagioclase (London 1992). Although cerium sequestration can occur into epidote group minerals (Glorie *et al.* 2019), this process appears minimal in the Johnston Complex given the absence of primary epidote group minerals or allanite (Fig. 2).

Sha and Chappell (1999) demonstrated that apatites in S-type and I-type granites show a chondrite-normalized depletion in Th and LREEs and, therefore, a shallower slope, which flattens with increasing atomic mass in REE plots (Fig. 7). Conversely, I-type granites can typically show a distinct enrichment in the LREEs and heavy REEs compared with U and the MREEs – a trend not evident in apatite from the Johnston Complex. Instead, the apatite has a negatively sloping REE trend with a moderate negative Eu anomaly of 0.35 and a mean $(Ce/Yb)_{cn}$ of 7.3, typical of apatite grains derived from evolved granitoids (Fig. 7) (Sha and Chappell 1999; Belousova *et al.* 2002*b*; Chu *et al.* 2009). Accordingly, the Johnston Complex apatite falls within the range of S-type granites compiled by O'Sullivan *et al.* (2020) (Fig. 7). The mineralogy of the Johnston Complex is also consistent with an S-type source, including apatite being relatively abundant (*c.* 0.20% modal abundance) and an absence of diagnostic minerals for I-type granites, such as allanite and magnetite (Chappell and White 2001). The predominant association of zircon within altered mafic minerals (chlorite and hornblende) in the Johnston Complex (Fig. 3) is also consistent with an S-type classification (Clemens *et al.* 2016).

Continental arc granitoids, such as the Johnston Complex, typically form by melting pre-existing crust, with potential input from juvenile material (Hawkesworth *et al.* 2010). I-type felsic melts can transition to a more peraluminous composition following assimilation with material derived from subduction, such as greywackes and shales (Chappell and White 2001). Extensive continental collision and orogenesis, associated with the assembly of Gondwana, were posited to have led to the uplift and production of giant turbidite fans (Zhu *et al.* 2020). The erosion of the uplifted hinterland supported the prolonged delivery of supracrustal detritus via subduction-related erosion followed by transfer to the upper plate. Our data suggest that the Johnston Complex, an S-type granite from a peri-Gondwanan terrane, is a consequence of this process.

Coupled apatite–zircon analyses in S-type granitoids

Obtaining primary magmatic crystallization ages can be challenging for S-type granites due to the common presence of inherited zircons, with difficulties in definitively identifying neoblastic growth in such rocks (Collins *et al.* 2021; Kelsey *et al.* 2022). Differentiating primary v. inherited zircon has important implications for accurate terrane classification, where zircon U–Pb crystallization ages are often the key discrimination or association parameter between disparate inliers (Pharaoh and Carney 2000; Schofield *et al.* 2016).

Given solubility considerations, apatite is much less likely to be an inherited phase in felsic melts than zircon (Wolf and London 1994). Where both zircon and apatite yield similar crystallization

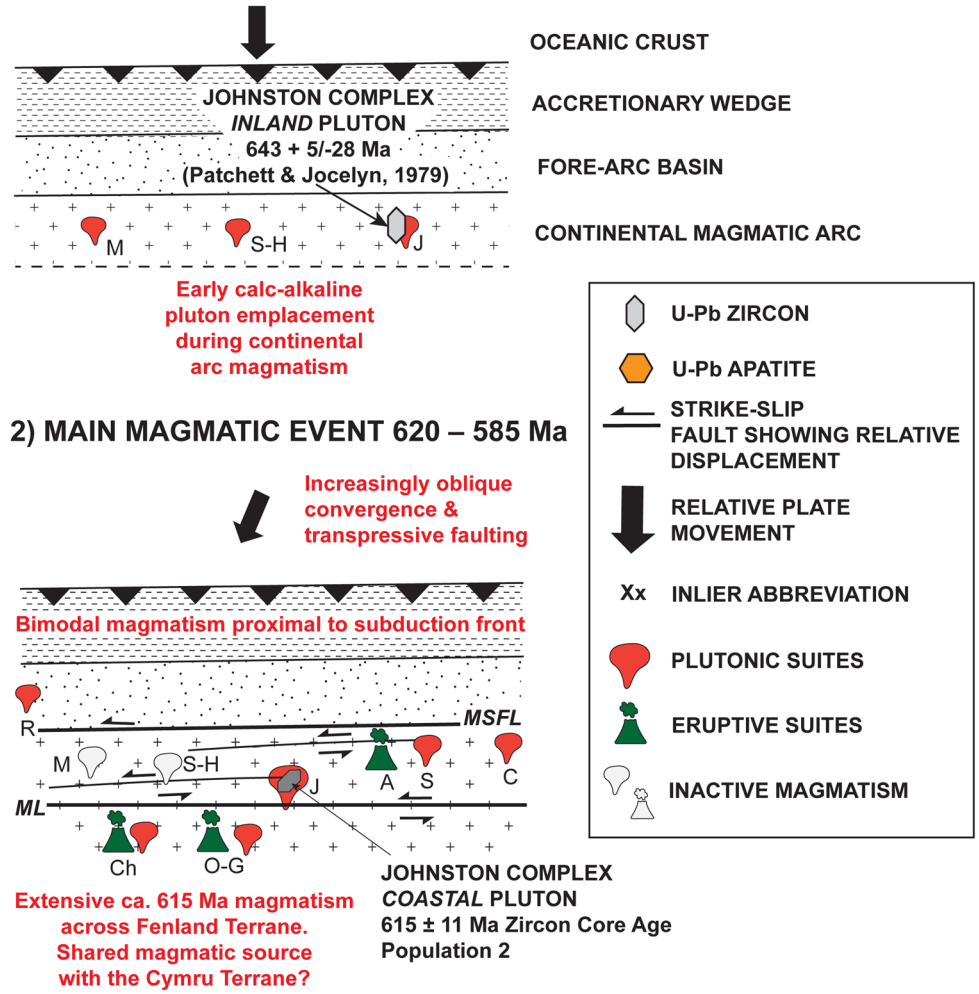

Fig. 9. Schematic model showing the late Neoproterozoic evolution of the Johnston Complex within the East Avalonian tectonic regime. A, Arfon Group; B, Anglesey blueschists; BG, Bwlch Gwyn Tuff; BV, Benton Volcanic Group; C, Coedana Complex; Ch, Charnian Supergroup; J, Johnston Complex; ML, Malverns Lineament; MSFS, Menai Strait Fault System; O-G, Orton and Glinton boreholes; P, Pebidian Supergroup; R, Rosslare Complex; S, Sarn Complex; S-H, Stanner–Hanter Complex; U-E-L, Uriconian volcanics; Ercall granophyre, Longmyndian Supergroup; WBFS, Welsh Borderland Fault System; WH, Warren House Volcanics. Model adapted after Horak *et al.* (1996) and Pharaoh and Carney (2000).

ages, and the host rock shows little evidence of recrystallization, this provides a compelling case for coeval magmatic growth. Coeval ages for both minerals also imply rapid cooling (i.e. shallow epizonal emplacement) through the radiogenic Pb closure temperature of both minerals (zircon ≥900°C and apatite ≥350°C) (Fig. 4) (Chew and Spikings 2021).

Apatite and zircon ages at *c.* 570 Ma for the Johnston Complex imply that calc-alkaline magmatism was ongoing during the final stages of Eastern Avalonian arc magmatism in the Cymru Terrane (Woodcock *et al.* 2012). Across the inliers of southern Britain, an absence of calc-alkaline magmatism after *c.* 570 Ma has been attributed to the increasingly oblique convergence of East Avalonia with Laurentia and the detachment of the coherent geology into tectonic slivers and subsequent terrane dispersal (Fig. 9) (Horak *et al.* 1996; Woodcock *et al.* 2012). The rapid cooling of the Johnston Complex at *c.* 570 Ma and its low metamorphic grade is consistent with structurally controlled emplacement into the shallow crust. Increasing rates of oblique convergence and transpression along strike-slip faults have been proposed to reduce the geothermal gradient of the mid- to upper crustal sections (Alvarado *et al.* 2016; Collett *et al.* 2019). Hence the 570 Ma age of the Johnston Complex is consistent with dispersal of the Eastern Avalonian Terrane along the subduction front (Woodcock *et al.* 2012). During this process, strike-slip faults would have provided conduits for melt emplacement and crystallization of the Johnston Complex at shallow epizonal depths (Murphy *et al.* 2022).

In addition, these new data imply that the Johnston Complex underwent minimal thermal disturbance following magmatic crystallization at *c.* 570 Ma. The U–Pb closure temperature of apatite is highly dependent on microstructures, grain size and cooling rates. Consequently, the reported closure temperatures range between 350 and 600°C (Chew and Spikings 2015; Kirkland *et al.* 2018). Nonetheless, apatite U–Pb ages typically represent metamorphic perturbances under mid- to upper crustal conditions or protracted cooling through the closure temperature range (Chew and Spikings 2015; Kirkland *et al.* 2018; Gillespie *et al.* 2022). The similarity between apatite and zircon U–Pb ages implies that the Johnston Complex cannot have resided at temperatures ≥350°C for a protracted period. Rather, the isotopic data imply rapid cooling through the U–Pb closure temperatures of both minerals. Rapid cooling at a relatively shallow depth of emplacement is consistent with the coeval crystallization of apatite and zircon within this constituent body of the Johnston Complex (Fig. 1).

K–Ar hornblende data from another coastal outcrop of the Johnston Complex have yielded *c.* 624–612 Ma ages and biotite from the Dutch Gin series, a so-called metre-scale band of localized deformation at the western margin of the Johnston Complex, yields a K–Ar date of *c.* 612 Ma (Thorpe 1979). The relatively lower closure temperature of the K–Ar system in both minerals (300–600°C) (Harrison 1982) further suggests that the Johnston Complex experienced minimal post-magmatic thermal perturbations. The Johnston Complex is now bound within a Variscan thrust zone and was also emplaced prior to the Caledonian Orogeny, but neither tectonic event caused extensive metamorphism of the complex (Thorpe 1972; Patchett and Jocelyn 1979). Indeed, across the Neoproterozoic rocks of SW Wales, metamorphism is limited to prehnite–pumpellyite facies (Fig. 1) (Thorpe 1972).

Zircon Lu–Hf: a Mesoproterozoic source melt?

The zircon εHf data for *c.* 570 Ma crystals (population 1) forms a broadly sub-chondritic cluster, with a mean εHf of −0.41 ± 1.38. The older *c.* 615 Ma (population 2) cores have εHf values that are not significantly different (Fig. 5), suggesting that both magmatic episodes were derived from compositionally similar sources (at least in terms of the Lu/Hf ratio) that did not undergo significant evolution or modification during the *c.* 615–570 Ma interval.

A Lu/Hf ratio of 0.05 was chosen to reflect a felsic source for the parental melt of the Johnston Complex, consistent with other S-type Proterozoic granitoids from the database compiled by Bea *et al.* (2018). Two-stage depleted mantle Lu–Hf model ages (T^2_{DM}) imply late Mesoproterozoic 1011–1892 Ma crust-extraction dates, with a mean T^2_{DM} of 1521 Ma. Model ages, especially in the case of S-type granitoids, may only provide a minimum age for the oldest component within a mixed magma. Nonetheless, the zircon Hf isotopic signature, with a source crustal residence time of at least 800–500 Ma, is similar to other Avalonian granitoids (Fig. 6) (Pollock *et al.* 2015; Henderson *et al.* 2016; Schofield *et al.* 2016).

A whole-rock εNd value of −1.8 with a T^2_{DM} of 1437 Ma was reported for the Johnston Complex from the inland outcrop (Schofield *et al.* 2016). Along with the Lu–Hf T^2_{DM} for zircon reported here, these data imply variable degrees of crustal contamination. Complementary εHf data from Western Avalonia granitoids yield analogous late Mesoproterozoic T^2_{DM} ages, implying a similar source for most Avalonian microcontinental blocks during the late Neoproterozoic (Fig. 6) (Willner *et al.* 2013; Pollock *et al.* 2015; Henderson *et al.* 2016).

Although localized areas of considerably older Proterozoic ≥1.6 Ga crust in West Avalonia have been inferred by εHf data (Willner *et al.* 2013; Pollock *et al.* 2015; Henderson *et al.* 2016), there is no evidence of similarly ancient crust based on the sparse Lu–Hf dataset for the Cymru Terrane. Nonetheless, the presence of older, mid-Proterozoic crustal components within the Cymru Terrane is implied by Sm–Nd model ages of *c.* >1.35 Ga for the Parwyd Gneisses and Sarn Granites (Fig. 1) (McIlroy and Horak 2006). Other areas show more definitive evidence of older underlying crust. For example, the Malverns Complex (Fig. 1) has yielded inherited zircon age maxima of *c.* 1.6 Ga and whole-rock Sm–Nd model ages of *c.* 1.6–1.4 Ga (Murphy *et al.* 2000; McIlroy and Horak 2006). Such older crustal components provide an important distinction between the Cymru and Wrekin terranes, in which the latter appears to incorporate an older crustal component.

Zircon data from other East Avalonian lithologies also show similar εHf patterns to the Johnston Complex. For example, zircon grains from the Stavelot–Venn Massif of East Avalonia imply felsic melt generation from a chondritic source of similar age and composition to the Johnston Complex (Fig. 6) (Willner *et al.* 2013). Hence εHf data from the Johnston Complex, when considered with data from other terranes, support the interpretation that Avalonian terranes formed from a relatively uniform Neoproterozoic continental arc system with a broadly chondritic melt source (Fig. 6) (Pollock *et al.* 2015) variably contaminated with older Meso- to Paleoproterozoic crust (e.g. the Wrekin Terrane) (Thorpe *et al.* 1984). This contamination could represent localized input into the subduction system of allochthonous structurally emplaced older crust during the Proterozoic (Pollock *et al.* 2015).

Conclusions

New time-constrained (U–Pb) isotopic (Lu–Hf) and trace element data from the Johnston Complex, SW Wales help to constrain magmatism in East Avalonia during the late Neoproterozoic. We report ages for a coastal pluton of the Johnston Complex from coeval apatite and zircon at 570 ± 3 Ma. Combined with a previously reported age of *c.* 643 Ma for an inland component, we demonstrate that the Johnston Complex is a composite suite of quartz diorite plutons along its *c.* 20 km length. Our data necessitate that calc-alkaline igneous activity was ongoing until *c.* 570 Ma in East Avalonia.

Apatite and zircon geochemistry provide complementary insights into late Neoproterozoic magmatism in southern Britain. Zircon trace elements demonstrate an oxidized calc-alkaline source magma typical of an ensialic subduction belt setting for the Johnston Complex. A sedimentary component within the melt is revealed through apatite trace element profiles, consistent with voluminous S-type granitoid production during the assembly of Gondwana. εHf values imply a broadly chondritic source melt for both zircon populations with a mean T^2_{DM} of 1.5 Ga.

Classification of the Precambrian terranes of southern Britain has primarily been facilitated through correlating geochemical

signatures, structural relationships and Nd (model) ages. Generally, sparse U–Pb magmatic crystallization dates have underpinned associations of otherwise disparate lithologies into unified terranes. Given this approach, the work presented here offers a cautionary note. On the kilometre scale, the Johnston Complex varies in age by more than *c.* 40 Ma (Fig. 3). Although individual zircon grains trace a multi-stage history with components at *c.* 615 and 570 Ma, the combined zircon–apatite approach gives confidence in magmatic age assignment and facilitates terrane association in partially obscured basement areas. Thus, in situations when the closure temperature of Pb in apatite has not been exceeded, the application of combined zircon and apatite geochronology may remove some of the ambiguity related to zircon inheritance when dating rocks.

Scientific editing by Yildirim Dilek

Acknowledgements The authors thank Bradley McDonald and Noreen Evans for assistance with the LA-ICP-MS data collection. We thank Brendan Murphy and Damian Nance for reviews that improved this work and Yildirim Dilek for facilitating a constructive review process.

Author contributions **AJIC**: formal analysis (lead), visualization (lead), writing – original draft (lead); **CLK**: conceptualization (lead), funding acquisition (lead), resources (lead), supervision (lead), writing – review and editing (lead); **SG**: funding acquisition (equal), supervision (supporting), writing – review and editing (supporting).

Funding This work was funded by an Australian Research Council Discovery Project (DP200101881). The instruments in the John deLaeter Centre, Curtin University, were funded via AuScope, the Australian Education Investment Fund, the National Collaborative Research Infrastructure Strategy and the Australian Government.

Competing interests The authors declare that they have no known competing financial interests or personal relationships that could have appeared to influence the work reported in this paper.

Data availability All data generated or analysed during this study are included in this published article (and if present, its supplementary information files).

References

Alvarado, A., Audin, L. *et al.*. 2016. Partitioning of oblique convergence in the Northern Andes subduction zone: migration history and the present-day boundary of the North Andean Sliver in Ecuador. *Tectonics*, **35**, 1048–1065, https://doi.org/10.1002/2016TC004117

Azadbakht, Z., Lentz, D. and McFarlane, C. 2018. Apatite chemical compositions from Acadian-related granitoids of New Brunswick, Canada: implications for petrogenesis and metallogenesis. *Minerals*, **8**, https://doi.org/10.3390/min8120598

Bacon, C.R. 1989. Crystallization of accessory phases in magmas by local saturation adjacent to phenocrysts. *Geochimica et Cosmochimica Acta*, **53**, 1055–1066, https://doi.org/10.1016/0016-7037(89)90210-X

Baker, J.W. 1982. The Precambrian of south-west Dyfed, south-west Wales. *In*: Bassett, M.G. (ed.) *Geological Excursions in Dyfed, South-West Wales*. National Museum of Wales, 15–25.

Bea, F., Montero, P., Molina, J.F., Scarrow, J.H., Cambeses, A. and Moreno, J.A. 2018. Lu–Hf ratios of crustal rocks and their bearing on zircon Hf isotope model ages: the effects of accessories. *Chemical Geology*, **484**, 179–190, https://doi.org/10.1016/j.chemgeo.2017.11.034

Beckinsale, R.D., Evans, J.A., Thorpe, R.S., Gibbons, W. and Harmon, R.S. 1984. Rb–Sr whole-rock isochron ages, $\delta^{18}O$ values and geochemical data for the Sarn Igneous Complex and the Parwyd gneisses of the Mona Complex of Llŷn, N Wales. *Journal of the Geological Society, London*, **141**, 701–709, https://doi.org/10.1144/gsjgs.141.4.0701

Belousova, E., Griffin, W., O'Reilly, S.Y. and Fisher, N. 2002*a*. Igneous zircon: trace element composition as an indicator of source rock type. *Contributions to Mineralogy and Petrology*, **143**, 602–622, https://doi.org/10.1007/s00410-002-0364-7

Belousova, E., Griffin, W., O'Reilly, S.Y. and Fisher, N. 2002*b*. Apatite as an indicator mineral for mineral exploration: trace-element compositions and their relationship to host rock type. *Journal of Geochemical Exploration*, **76**, 45–69, https://doi.org/10.1016/S0375-6742(02)00204-2

Bénard, A., Klimm, K. *et al.*. 2018. Oxidising agents in sub-arc mantle melts link slab devolatilisation and arc magmas. *Nature Communications*, **9**, 3500, https://doi.org/10.1038/s41467-018-05804-2

Bevins, R., Pharaoh, T., Cope, J. and Brewer, T. 1995. Geochemical character of Neoproterozoic volcanic rocks in southwest Wales. *Geological Magazine*, **132**, 339–349, https://doi.org/10.1017/S0016756800013649

Bloxam, T.W. and Dirk, M.H.J. 1988. The petrology and geochemistry of the St. David's granophyre and the Cwm Bach rhyolite, Pembrokeshire, Dyfed. *Mineralogical Magazine*, **52**, 563–575, https://doi.org/10.1180/minmag.1988.052.368.02

Boynton, W.V. 1984. Cosmochemistry of the rare earth elements: meteorite studies. *In*: Henderson, P. (ed.) *Developments in Geochemistry*. Elsevier, 63–114, https://doi.org/10.1016/B978-0-444-42148-7.50008-3

Cantrill, T.C., Dixon, E.E.L., Thomas, H.W. and Jones, O.T. 1916. *The Geology of the South Wales Coalfield, Part XII, The Country Around Milford*. His Majesty's Stationery Office.

Cawood, P.A., Martin, E.L., Murphy, J.B. and Pisarevsky, S.A. 2021. Gondwana's interlinked peripheral orogens. *Earth and Planetary Science Letters*, **568**, 117057, https://doi.org/10.1016/j.epsl.2021.117057

Chappell, B.W. and White, A.J.R. 2001. Two contrasting granite types: 25 years later. *Australian Journal of Earth Sciences*, **48**, 489–499, https://doi.org/10.1046/j.1440-0952.2001.00882.x

Chew, D.M. and Spikings, R.A. 2015. Geochronology and thermochronology using apatite: time and temperature, lower crust to surface. *Elements*, **11**, 189–194, https://doi.org/10.2113/gselements.11.3.189

Chew, D.M. and Spikings, R.A. 2021. Apatite U–Pb thermochronology: a review. *Minerals*, **11**, 1095, https://doi.org/10.3390/min11101095

Chu, M.F., Wang, K.L., Griffin, W., Chung, S.L., O'Reilly, S.Y., Pearson, D.G. and Iizuka, Y. 2009. Apatite composition: tracing petrogenetic processes in Transhimalayan granitoids. *Journal of Petrology*, **50**, 1829–1855, https://doi.org/10.1093/petrology/egp054

Clemens, J.D., Buick, I.S. and Kisters, A.F.M. 2016. The Donkerhuk batholith, Namibia: a giant S-type granite emplaced in the mid crust, in a fore-arc setting. *Journal of the Geological Society, London*, **174**, 157–169, https://doi.org/10.1144/jgs2016-028

Collett, C.M., Duvall, A.R., Flowers, R.M., Tucker, G.E. and Upton, P. 2019. The timing and style of oblique deformation within New Zealand's Kaikōura ranges and Marlborough fault system based on low-temperature thermochronology. *Tectonics*, **38**, 1250–1272, https://doi.org/10.1029/2018TC005268

Collins, W.J., Murphy, J.B., Blereau, E. and Huang, H.Q. 2021. Water availability controls crustal melting temperatures. *Lithos*, **402–403**, 106351, https://doi.org/10.1016/j.lithos.2021.106351

Compston, W., Wright, A.E. and Toghill, P. 2002. Dating the Late Precambrian volcanicity of England and Wales. *Journal of the Geological Society, London*, **159**, 323–339, https://doi.org/10.1144/0016-764901-010

Dumitru, T.A. 2016. A new zircon concentrating table designed for geochronologists. *AGU Fall Meeting Abstracts*, **2016**, V23A–V2956A.

Elburg, M.A. 1996. U–Pb ages and morphologies of zircon in micrograniteoid enclaves and peraluminous host granite: evidence for magma mingling. *Contributions to Mineralogy and Petrology*, **123**, 177–189, https://doi.org/10.1007/s004100050149

Erdmann, S., Wodicka, N., Jackson, S. and Corrigan, D. 2013. Zircon textures and composition: refractory recorders of magmatic volatile evolution? *Contributions to Mineralogy and Petrology*, **165**, 45–71, https://doi.org/10.1007/s00410-012-0791-z

Fisher, C.M., Vervoort, J.D. and DuFrane, S.A. 2014*a*. Accurate Hf isotope determinations of complex zircons using the 'laser ablation split stream' method. *Geochemistry, Geophysics, Geosystems*, **15**, 121–139, https://doi.org/10.1002/2013GC004962

Fisher, C.M., Vervoort, J.D. and Hanchar, J.M. 2014*b*. Guidelines for reporting zircon Hf isotopic data by LA-MC-ICPMS and potential pitfalls in the interpretation of these data. *Chemical Geology*, **363**, 125–133, https://doi.org/10.1016/j.chemgeo.2013.10.019

Gillespie, J., Kirkland, C.L., Kinny, P.D., Simpson, A., Glorie, S. and Rankenburg, K. 2022. Lu–Hf, Sm–Nd, and U–Pb isotopic coupling and decoupling in apatite. *Geochimica et Cosmochimica Acta*, **338**, 121–135, https://doi.org/10.1016/j.gca.2022.09.038

Glorie, S., Jepson, G. *et al.*. 2019. Thermochronological and geochemical footprints of post-orogenic fluid alteration recorded in apatite: implications for mineralisation in the Uzbek Tian Shan. *Gondwana Research*, **71**, 1–15, https://doi.org/10.1016/j.gr.2019.01.011

Grimes, C.B., Wooden, J.L., Cheadle, M.J. and John, B.E. 2015. 'Fingerprinting' tectono-magmatic provenance using trace elements in igneous zircon. *Contributions to Mineralogy and Petrology*, **170**, 46, https://doi.org/10.1007/s00410-015-1199-3

Harrison, T.M. 1982. Diffusion of ^{40}Ar in hornblende. *Contributions to Mineralogy and Petrology*, **78**, 324–331, https://doi.org/10.1007/BF00398927

Hawkesworth, C.J., Dhuime, B., Pietranik, A.B., Cawood, P.A., Kemp, A.I.S. and Storey, C.D. 2010. The generation and evolution of the continental crust. *Journal of the Geological Society, London*, **167**, 229–248, https://doi.org/10.1144/0016-76492009-072

Henderson, B.J., Collins, W.J., Murphy, J.B., Gutierrez-Alonso, G. and Hand, M. 2016. Gondwanan basement terranes of the Variscan–Appalachian orogen: Baltican, Saharan and West African hafnium isotopic fingerprints in Avalonia,

Iberia and the Armorican terranes. *Tectonophysics*, **681**, 278–304, https://doi.org/10.1016/j.tecto.2015.11.020

Horak, J., Doig, R., Evans, J. and Gibbons, W.D. 1996. Avalonian magmatism and terrane linkage: new isotopic data from the Precambrian of North Wales. *Journal of the Geological Society, London*, **153**, 91–99, https://doi.org/10.1144/gsjgs.153.1.0091

Jackson, S.E., Pearson, N.J., Griffin, W.L. and Belousova, E.A. 2004. The application of laser ablation-inductively coupled plasma-mass spectrometry to in situ U–Pb zircon geochronology. *Chemical Geology*, **211**, 47–69, https://doi.org/10.1016/j.chemgeo.2004.06.017

Jochum, K.P., Nohl, U., Herwig, K., Lammel, E., Stoll, B. and Hofmann, A.W. 2005. GeoReM: a new geochemical database for reference materials and isotopic standards. *Geostandards and Geoanalytical Research*, **29**, 333–338, https://doi.org/10.1111/j.1751-908X.2005.tb00904.x

Kelsey, D.E., Wingate, M. *et al.*. 2022. *Crystalline Basement Beneath the Eastern Canning Basin at the Top Up Rise Prospect*. Geological Survey of Western Australia.

Kirkland, C.L., Hollis, J., Danišík, M., Petersen, J., Evans, N.J. and McDonald, B.J. 2017. Apatite and titanite from the Karrat Group, Greenland; implications for charting the thermal evolution of crust from the U–Pb geochronology of common Pb-bearing phases. *Precambrian Research*, **300**, 107–120, https://doi.org/10.1016/j.precamres.2017.07.033

Kirkland, C.L., Yakymchuk, C., Szilas, K., Evans, N., Hollis, J., McDonald, B. and Gardiner, N.J. 2018. Apatite: a U–Pb thermochronometer or geochronometer? *Lithos*, **318–319**, 143–157, https://doi.org/10.1016/j.lithos.2018.08.007

London, D. 1992. Phosphorus in S-type magmas: the P_2O_5 content of feldspars from peraluminous granites, pegmatites, and rhyolites. *American Mineralogist*, **77**, 126–145.

Marsh, J.H., Jørgensen, T.R.C., Petrus, J.A., Hamilton, M.A. and Mole, D.R. 2019. U–Pb, trace element, and hafnium isotope composition of the Maniitsoq zircon: A potential new Archean zircon reference material. Goldschmidt, Barcelona, 18–23 August 2019, https://goldschmidtabstracts.info/2019/2161.pdf

McDowell, F., McIntosh, W. and Farley, K. 2005. A precise ^{40}Ar–^{39}Ar reference age for the Durango apatite (U–Th)/He and fission-track dating standard. *Chemical Geology*, **214**, 249–263, https://doi.org/10.1016/j.chemgeo.2004.10.002

McIlroy, D. and Horak, J. 2006. The Neoproterozoic of England and Wales. *In*: Brenchly, P.J. and Rawson, P.F. (eds) *The Geology of England and Wales*. Geological Society of London, 9–24.

Meert, G.J. and Van Der Voo, R. 1997. The assembly of Gondwana 800–550 Ma. *Journal of Geodynamics*, **23**, 223–235, https://doi.org/10.1016/S0264-3707(96)00046-4

Miller, J.S., Matzel, J.E.P., Miller, C.F., Burgess, S.D. and Miller, R.B. 2007. Zircon growth and recycling during the assembly of large, composite arc plutons. *Journal of Volcanology and Geothermal Research*, **167**, 282–299, https://doi.org/10.1016/j.jvolgeores.2007.04.019

Morel, M.L.A., Nebel, O., Nebel-Jacobsen, Y., Miller, J. and Vroon, P.Z. 2008. Hafnium isotope characterization of the GJ-1 zircon reference material by solution and laser-ablation MC-ICPMS. *Chemical Geology*, **255**, 231–235, https://doi.org/10.1016/j.chemgeo.2008.06.040

Murphy, J.B., Strachan, R.A., Nance, R.D., Parker, K.D. and Fowler, M.B. 2000. Proto-Avalonia: a 1.2–1.0 Ga tectonothermal event and constraints for the evolution of Rodinia. *Geology*, **28**, 1071–1074, https://doi.org/10.1130/0091-7613(2000)28<1071:PAGTEA>2.0.CO;2

Murphy, J.B., Collins, W.J. and Archibald, D.B. 2022. Logan Medallist 7. Appinite complexes, granitoid batholiths and crustal growth: a conceptual model. *Geoscience Canada*, **49**, 237–249, https://doi.org/10.12789/geocanj.2022.49.191

Nance, R.D., Murphy, J.B. *et al.* 2008. Neoproterozoic-early Palaeozoic tectonostratigraphy and palaeogeography of the peri-Gondwanan terranes: Amazonian v. West African connections. *Geological Society, London, Special Publications*, **297**, 345–383, https://doi.org/10.1144/SP297.17

Noble, S.R., Tucker, R.D. and Pharaoh, T.C. 1993. Lower Palaeozoic and Precambrian igneous rocks from eastern England, and their bearing on late Ordovician closure of the Tornquist Sea: constraints from U–Pb and Nd isotopes. *Geological Magazine*, **130**, 835–846, https://doi.org/10.1017/S0016756800023190

O'Sullivan, G., Chew, D.M., Kenny, G., Henrichs, I. and Mulligan, D. 2020. The trace element composition of apatite and its application to detrital provenance studies. *Earth-Science Reviews*, **201**, https://doi.org/10.1016/j.earscirev.2019.103044

Patchett, P.J. and Jocelyn, J. 1979. U–Pb zircon ages for late Precambrian igneous rocks in South Wales. *Journal of the Geological Society, London*, **136**, 13–19, https://doi.org/10.1144/gsjgs.136.1.0013

Pharaoh, T.C. and Carney, J.N. 2000. Introduction to the Precambrian Rocks of England and Wales. *In*: Carney, J.N. (ed.) *Geological Conservation Review Series*. Joint Nature Conservation Committee, 3–15 and 127–136.

Pharaoh, T.C., Webb, P.C., Thorpe, R.S. and Beckinsale, R.D. 1987. Geochemical evidence for the tectonic setting of Late Proterozoic volcanic suites in Central England. *Geological Society, London, Special Publications*, **33**, 541–552, https://doi.org/10.1144/GSL.SP.1987.033.01.36

Pollock, J., Sylvester, P. and Barr, S.M. 2015. Lu–Hf zircon and Sm–Nd whole-rock isotope constraints on the extent of juvenile arc crust in Avalonia: examples from Newfoundland and Nova Scotia, Canada. *Canadian Journal of Earth Sciences*, **52**, 161–181, https://doi.org/10.1139/cjes-2014-0157

Rino, S., Kon, Y., Sato, W., Maruyama, S., Santosh, M. and Zhao, D. 2008. The Grenvillian and Pan-African orogens: world's largest orogenies through geologic time, and their implications on the origin of superplume. *Gondwana Research*, **14**, 51–72, https://doi.org/10.1016/j.gr.2008.01.001

Sano, Y., Terada, K. and Fukuoka, T. 2002. High mass resolution ion microprobe analysis of rare earth elements in silicate glass, apatite and zircon: lack of matrix dependency. *Chemical Geology*, **184**, 217–230, https://doi.org/10.1016/S0009-2541(01)00366-7

Schmitz, M.D., Bowring, S.A. and Ireland, T.R. 2003. Evaluation of Duluth Complex anorthositic series (AS3) zircon as a U–Pb geochronological standard: new high-precision isotope dilution thermal ionization mass spectrometry results. *Geochimica et Cosmochimica Acta*, **67**, 3665–3672, https://doi.org/10.1016/S0016-7037(03)00200-X

Schoene, B. and Bowring, S. 2006. U–Pb systematics of the McClure Mountain syenite: thermochronological constraints on the age of the $^{40}Ar/^{39}Ar$ standard MMhb. *Contributions to Mineralogy and Petrology*, **151**, 615–630, https://doi.org/10.1007/s00410-006-0077-4

Schofield, D., Millar, I.L., Wilby, P. and Evans, J. 2010. A new, high precision U–Pb date from the oldest known rocks in southern Britain. *Geological Magazine*, **147**, 145–150, https://doi.org/10.1017/S001675680999063X

Schofield, D., Potter, J., Barr, S.M., Horák, J.M., Millar, I.L. and Longstaffe, F.J. 2016. Reappraising the Neoproterozoic 'East Avalonian' terranes of southern Great Britain. *Gondwana Research*, **35**, 257–271, https://doi.org/10.1016/j.gr.2015.06.001

Sha, L.K. and Chappell, B.W. 1999. Apatite chemical composition, determined by electron microprobe and laser-ablation inductively coupled plasma mass spectrometry, as a probe into granite petrogenesis. *Geochimica et Cosmochimica Acta*, **63**, 3861–3881, https://doi.org/10.1016/S0016-7037(99)00210-0

Shen, B., Dong, L., Xiao, S. and Kowalewski, M. 2008. The Avalon explosion: evolution of Ediacara morphospace. *Science*, **319**, 81–84, https://doi.org/10.1126/science.1150279

Shields-Zhou, G.A., Porter, S. and Halverson, G.P. 2016. A new rock-based definition for the Cryogenian Period (circa 720–635 Ma). *Episodes*, **39**, 3–8, https://doi.org/10.18814/epiiugs/2016/v39i1/89231

Sláma, J., Košler, J. *et al.*. 2008. Plešovice zircon – a new natural reference material for U–Pb and Hf isotopic microanalysis. *Chemical Geology*, **249**, 1–35, https://doi.org/10.1016/j.chemgeo.2007.11.005

Stern, R.A., Bodorkos, S., Kamo, S.L., Hickman, A.H. and Corfu, F. 2009. Measurement of SIMS instrumental mass fractionation of Pb isotopes during zircon dating. *Geostandards and Geoanalytical Research*, **33**, 145–168, https://doi.org/10.1111/j.1751-908X.2009.00023.x

Strachan, R.A., Nance, R.D., Dallmeyer, R., D'Lemos, R.S., Murphy, J.B. and Watt, G.R. 1996. Late Precambrian tectonothermal evolution of the Malverns Complex. *Journal of the Geological Society, London*, **153**, 589–600, https://doi.org/10.1144/gsjgs.153.4.0589

Strachan, R.A., Collins, A., Buchan, C., Nance, R.D., Murphy, J.B. and D'Lemos, R.S. 2007. Terrane analysis along a Neoproterozoic active margin of Gondwana: insights from U–Pb zircon geochronology. *Journal of the Geological Society, London*, **164**, 57–60, https://doi.org/10.1144/0016-76492006-014

Thompson, J., Meffre, S. *et al.*. 2016. Matrix effects in Pb/U measurements during LA-ICP-MS analysis of the mineral apatite. *Journal of Analytical Atomic Spectrometry*, **31**, 1206–1215, https://doi.org/10.1039/c6ja00048g

Thorpe, R.S. 1972. Possible subduction origin for two Pre-Cambrian calc-alkaline plutonic complexes from southern Britain. *GSA Bulletin*, **83**, 36–63, https://doi.org/10.1130/0016-7606(1972)83[3663:PSZOFT]2.0.CO;2

Thorpe, R.S. 1979. Late Precambrian igneous activity in Southern Britain. *Geological Society, London, Special Publications*, **8**, 579–584, https://doi.org/10.1144/GSL.SP.1979.008.01.68

Thorpe, R.S., Beckinsale, R.D., Patchett, P.J., Piper, J.D.A., Davies, G.R. and Evans, J.A. 1984. Crustal growth and late Precambrian–early Palaeozoic plate tectonic evolution of England and Wales. *Journal of the Geological Society, London*, **141**, 521–536, https://doi.org/10.1144/gsjgs.141.3.0521

Tucker, R.D. and Pharaoh, T.C. 1991. U–Pb zircon ages for Late Precambrian igneous rocks in southern Britain. *Journal of the Geological Society, London*, **148**, 435–443, https://doi.org/10.1144/gsjgs.148.3.0435

Valley, J.W., Cavosie, A.J. *et al.*. 2014. Hadean age for a post-magma-ocean zircon confirmed by atom-probe tomography. *Nature Geoscience*, **7**, 219–223, https://doi.org/10.1038/ngeo2075

Wiedenbeck, M., Allé, P. *et al.*. 1995. Three natural zircon standards for U–Th–Pb, Lu–Hf, trace element and REE analyses. *Geostandards Newsletter*, **19**, 1–23, https://doi.org/10.1111/j.1751-908X.1995.tb00147.x

Willner, A.P., Barr, S.M., Gerdes, A., Massonne, H.J. and White, C.E. 2013. Origin and evolution of Avalonia: evidence from U–Pb and Lu–Hf isotopes in zircon from the Mira terrane, Canada, and the Stavelot-Venn Massif, Belgium. *Journal of the Geological Society, London*, **170**, 769–784, https://doi.org/10.1144/jgs2012-152

Wolf, M.B. and London, D. 1994. Apatite dissolution into peraluminous haplogranitic melts: an experimental study of solubilities and mechanisms. *Geochimica et Cosmochimica Acta*, **58**, 4127–4145, https://doi.org/10.1016/0016-7037(94)90269-0

Woodcock, N., Holdsworth, R.E. and Strachan, R.A. 2012. *Geological History of Britain and Ireland*, 2nd edn. Wiley-Blackwell.

Woodhead, J.D. and Hergt, J.M. 2005. A preliminary appraisal of seven natural zircon reference materials for in situ Hf isotope determination. *Geostandards and Geoanalytical Research*, **29**, 183–195, https://doi.org/10.1111/j.1751-908X.2005.tb00891.x

Woodhead, J.D., Hergt, J.M., Shelley, M., Eggins, S. and Kemp, R. 2004. Zircon Hf-isotope analysis with an excimer laser, depth profiling, ablation of complex geometries, and concomitant age estimation. *Chemical Geology*, **209**, 121–135, https://doi.org/10.1016/j.chemgeo.2004.04.026

Zhu, Z., Campbell, I.H., Allen, C.M. and Burnham, A.D. 2020. S-type granites: their origin and distribution through time as determined from detrital zircons. *Earth and Planetary Science Letters*, **536**, 116140, https://doi.org/10.1016/j.epsl.2020.116140